

SchWARMA: A model-based approach for time-correlated noise in quantum circuits

Kevin Schultz, Gregory Quiroz, Paraj Titum, and B.D. Clader

Johns Hopkins University Applied Physics Laboratory

11100 Johns Hopkins Road, Laurel, MD, 20723, USA

(Dated: October 12, 2020)

Temporal noise correlations are ubiquitous in quantum systems, yet often neglected in the analysis of quantum circuits due to the complexity required to accurately characterize and model them. Autoregressive moving average (ARMA) models are a well-known technique from time series analysis that model time correlations in data. By identifying the space of completely positive trace preserving (CPTP) quantum operations with a particular matrix manifold, we generalize ARMA models to the space of CPTP maps to parameterize and simulate temporally correlated noise in quantum circuits. This approach, denoted Schrödinger Wave ARMA (SchWARMA), provides a natural path for generalization of classic techniques from signal processing, control theory, and system identification for which ARMA models and linear systems are essential. This enables the broad theory of classical signal processing to be applied to quantum system simulation, characterization, and noise mitigation.

Introduction—The circuit model of quantum computing [1–3] has been used extensively to prove algorithmic speedups [4–6] as well as the theory of fault-tolerant quantum computing [7–9]. This model makes an implicit assumption that a quantum computation can be broken up into a series of (possibly imperfect) incremental gates. This assumption generally implies that noise processes are uncorrelated in space and time. However, the presence of time-correlated noise is well established in actual physical systems, e.g., $1/f^\alpha$ noise in superconducting qubits [10–14]. Characterization of such noise processes typically involves non-parametric reconstructions of the entire noise spectra [11, 15–20] requiring a large number of experiments. Furthermore, outside of a few closed-form cases, there is no more efficient way of forward simulating the dynamics of time-correlated noise short of brute-force numerical integration of the stochastic Liouville equation [21] for the entire circuit. The time step for such a simulation is typically orders of magnitude smaller than the nominal “gate duration,” resulting in a large number of matrix operations per gate. This approach is computationally very expensive, which has prevented much in the way of analysis of time-correlations in quantum circuits beyond a few qubits.

In this Letter, we introduce a model of temporally correlated noise that allows the wide-ranging field of classical time-series analysis to be applied to noisy circuit simulation and quantum noise spectroscopy. Our model draws on the time series analysis technique of auto regressive moving average (ARMA) models [22, 23], allowing us to connect open quantum systems to discrete time linear systems theory and model-based spectrum estimation [24]. With simulation and estimation of noisy quantum dynamics in mind, we generalize ARMA models to the space of completely positive trace preserving (CPTP) maps, an approach we denote Schrödinger Wave ARMA (SchWARMA). We convey the efficacy and versatility of this method by providing a set of useful examples of temporally correlated noise-affected dynamics from quantum control and error correction; see supplement for extensions to adiabatic quantum computing.

SchWARMA has a natural connection to semi-classical

stochastic Hamiltonian noise in quantum systems, but is more general in that it can also model correlated errors in dissipative system-bath as in a stochastic form of Lindblad master equation [25]. In this sense, the errors considered here are fundamentally Markovian with respect to any quantum bath, as the dynamics produced are correlated yet remain completely positive (CP) divisible [26]. This is a key requirement of the ability to separate a circuit into an ideal and error portions, an assumption in many characterization protocols, e.g., randomized benchmarking [27] or gate-set-tomography [28–30], both of which also assume errors are uncorrelated in time. Techniques such as [31] that seek to model non-Markovian quantum dynamics are fundamentally different from this noisy-circuit approach, as non-CP error channels interspersed with perfect gates can produce non-physical states. That said, our technique can be generalized to simulate system-bath models of non-Markovian quantum dynamics at an obvious reduction of the number of qubits simulated, but we leave this to future work.

An ARMA model relates the output y_k , at discrete steps k , to a series of inputs x_k and prior outputs via [22, 23],

$$y_k = \underbrace{\sum_{i=1}^p a_i y_{k-i}}_{AR} + \underbrace{\sum_{j=0}^q b_j x_{k-j}}_{MA}. \quad (1)$$

The set $\{a_i\}$ defines the autoregressive portion of the model, and $\{b_j\}$ the moving average portion with p and $q+1$ elements of each set respectively. ARMA models (and their many generalizations [32]) are commonly used in classical time series analysis to parametrically define, estimate, and simulate time-correlated processes [23], and have wide-ranging applications all the way from actuarial science [33] to zoology [34].

We generalize ARMA models to CPTP maps by introducing *Stiefel* manifolds [35], which consist of matrices with orthonormal columns. The tangent space of these manifolds enable a natural connection to the mathematics of ARMA on Lie algebras (i.e., the tangent space to a Lie group) [36] and to the Lindblad form of the master equation. Using these relationships, we build a theory of ARMA models relevant for

quantum information processing that enables one to model temporally-correlated noise in a circuit-model formalism.

We begin by showing how CPTP maps are related to Stiefel manifolds. A CPTP map Φ operating on $N \times N$ density operators ρ can be expressed by $\Phi(\rho) = \sum_k M_k \rho M_k^\dagger$ where M_k are $N \times N$ complex matrices called Kraus operators [37] with $\sum_k M_k^\dagger M_k = I_N$. This form is not unique, but any CPTP map can be expressed using no more than N^2 Kraus operators [37]. Given K Kraus operators $\{M_k\}$, we define $\mathcal{S} = [M_1^\dagger, \dots, M_K^\dagger]^\dagger$, a $KN \times N$ matrix with orthonormal columns.

Complex $n \times m$ matrices ($n \geq m$) with orthonormal columns define a Stiefel manifold [35], denoted $V_m(\mathbb{C}^n)$. Thus, the $KN \times N$ matrix $\mathcal{S} \in V_N(\mathbb{C}^{KN})$ relates the Kraus operators of a quantum channel to points on the corresponding Stiefel manifold. In order to describe perturbations around this point on the manifold, we introduce the tangent space of $V_N(\mathbb{C}^{KN})$. The tangent vectors are given by matrices $X = \mathcal{S}A + \mathcal{S}_\perp B$ with A $N \times N$ skew-Hermitian, B $(KN-N) \times N$ arbitrary, and \mathcal{S}_\perp denotes an orthogonal complement to \mathcal{S} such that $[\mathcal{S} \mathcal{S}_\perp]$ is unitary [38]. An exponential map at \mathcal{S} maps X back to the manifold via

$$\exp_{\mathcal{S}}(X) = [\mathcal{S} \mathcal{S}_\perp] \exp \left(\begin{bmatrix} A & -B^\dagger \\ B & \mathbf{0} \end{bmatrix} \right) I_{KN,N} \quad (2)$$

where $I_{n,m}$ denotes the first m columns of the $n \times n$ identity matrix I_n , and $\mathbf{0}$ is a zero-matrix of appropriate dimension [38, Eq. (2.42)]. Therefore, this map provides a mechanism to generate new elements of $V_N(\mathbb{C}^{KN})$ for specific choices of matrices A, B and \mathcal{S}_\perp .

For quantum information applications, we typically describe a noisy quantum channel as a perturbation around some desired unitary operation U . This corresponds to choosing $\mathcal{S} = [U^\dagger, \mathbf{0}]^\dagger$, and provides a natural choice for $\mathcal{S}_\perp = [\mathbf{0}, I_{KN-N}]^\dagger$. The exponential map in Eq. (2) generates the perturbed quantum channel. The form of the map highlights a natural geometric interpretation: B is a block matrix of $K-1$ individual $N \times N$ matrices B_k , so r nonzero blocks result in CPTP maps with Kraus rank $K = 1+r$, except periodically at the initial point U . This also has a natural connection to the Lindblad master equation through the infinitesimal limit of Eq. (2) that yields the time-evolution of the system density matrix [39],

$$\dot{\rho} = -i[H, \rho] + \sum_{k=1}^K \left(B_k \rho B_k^\dagger - \frac{1}{2} \{B_k^\dagger B_k, \rho\} \right), \quad (3)$$

where $H = -A/i$.

We now generalize ARMA techniques to the evolution of CPTP maps. Consider a combination of L independent ARMA models with an upper index ℓ where $y_k^{(\ell)}$ denotes the output of the ℓ^{th} model at time step k , and so on for $a_i^{(\ell)}, b_j^{(\ell)}$, and $x_k^{(\ell)}$. As in standard ARMA, $x_k^{(\ell)}$ are independent zero-mean Gaussian random variables with unit variance (other distributions may be used, however). Let $X^{(\ell)}$ denote fixed elements of the tangent space of \mathcal{U}_k in $V_N(\mathbb{C}^{KN})$ corresponding

to the target unitary U_k . Then, we define the CPTP map output \mathcal{S}_k of a Schrödinger Wave ARMA (SchWARMA) model at time k via (c.f. [36, Eq. (2.20)])

$$y_k^{(\ell)} = \sum_{i=1}^{p^{(\ell)}} a_i^{(\ell)} y_{k-i}^{(\ell)} + \sum_{j=0}^{q^{(\ell)}} b_j^{(\ell)} x_{k-j}^{(\ell)} \quad (4a)$$

$$\mathcal{S}_k = \exp_{\mathcal{U}_k} \left(\sum_{\ell=1}^L y_k^{(\ell)} X^{(\ell)} \right). \quad (4b)$$

The \mathcal{S}_k can then be composed as CPTP maps to implement correlated noisy quantum dynamics.

The SchWARMA model provides a coarse-grained representation of time-correlations in a quantum channel. Specifically, it describes noisy quantum dynamics at discrete time steps (indexed by k in Eq. (4) and subsequent examples), such as at circuit gate locations. To our knowledge, the only other way to do this is using a Suzuki-Trotter method [40–43] to numerically solve the Liouville equation. This requires steps sizes much smaller than the fluctuation time-scale of the Hamiltonian such that $\Delta t \ll \|\partial H(t)/\partial t\|^{-1}$ [44]. For high-bandwidth noise or control pulses, this can require many time steps to accurately simulate the trajectory. SchWARMA, on the other hand, allows us to estimate the impact of the time-dependent noise as a error channel after a perfect gate. Thus, SchWARMA can provide significant advantage for simulating noisy quantum systems by allowing control and noise to be separated in the model, even in the presence of time-correlations. In the following, we discuss examples using SchWARMA models for dephasing and amplitude damping channels. In the supplement, we extend this to other cases such as the depolarizing channel, as well as continuously driven quantum systems [39].

Let us start by discussing an example of a SchWARMA model to simulate dephasing. Temporally correlated single-axis dephasing noise on a single qubit identity channel can be generated by setting $U = I_2$, $A = -i\sigma_z$, and $B = 0$, yielding $X = -i\sigma_z$, where we have suppressed the ℓ index, since only a single SchWARMA model is needed. This implies $N = 2$ and $K = 1$, corresponding to unitary dynamics on a qubit. Using Eqs. (2) and (4b), we obtain the map to apply at circuit location k , $\mathcal{S}_k = \exp(-i\sigma_z y_k)$. Clearly, this is a Z rotation with an angle given by a classical ARMA model. This can be straightforwardly generalized to the case of multi-axis noise using $L = 3$ underlying ARMA models and $X^{(j)} = -i\sigma_j$ for $j \in \{x, y, z\}$. The multi-axis nature of the noise yields the following set of CPTP maps, $\mathcal{S}_k = \exp(-i\sigma_x y_k^{(x)} - i\sigma_y y_k^{(y)} - i\sigma_z y_k^{(z)})$.

The SchWARMA model may also be used to simulate non-unitary channels such as the amplitude damping channel. In this case, the appropriate tangent space element is

$$X = \begin{bmatrix} \mathbf{0}_{2 \times 2} \\ B \end{bmatrix}, \text{ with } B = \begin{bmatrix} 0 & 1 \\ 0 & 0 \end{bmatrix}, \quad (5)$$

where the notation $\mathbf{0}_{m \times n}$ indicates a matrix of zeros with m

rows and n columns, $N = 2$, and $K = 2$. Using the definition for B in Eq. (5), S_k is given as,

$$S_k = \exp \left(y_k \begin{bmatrix} \mathbf{0}_{2 \times 2} & -B^\dagger \\ B & \mathbf{0}_{2 \times 2} \end{bmatrix} \right) I_{4,2}, \quad (6)$$

yielding a 4×2 sized matrix containing the two 2×2 Kraus operators. Since X in (5) has all zeros in the skew-symmetric A component, in this case the driving ARMA model $y_k \equiv |y_k| e^{i\angle y_k}$ can actually be complex-valued with $\angle y_k = \tan^{-1}(\text{Im } y_k / \text{Re } y_k)$ denoting the polar angle. Evaluating Eq. (6) yields the Kraus operators at step k ,

$$M_1^{(k)} = \begin{bmatrix} 1 & 0 \\ 0 & \cos |y_k| \end{bmatrix} \text{ and } M_2^{(k)} = \begin{bmatrix} 0 & e^{i\angle y_k} \sin |y_k| \\ 0 & 0 \end{bmatrix}. \quad (7)$$

Clearly, this SchWARMA model simulates an amplitude damping channel with a correlated, fluctuating decay rate. This model allows one to analyze temporal fluctuations that may exist in the decay rate of the qubit [45]. However, it does not consider time-dynamics associated with the system-bath interaction which is still assumed to happen on infinitely fast time-scales; see supplement for details [39].

We now demonstrate the utility of SchWARMA for analyzing correlated noise within a variety of domains relevant to quantum information processing. We first build from single-qubit examples in quantum noise spectroscopy and control, showing strong agreement with established theory. Then we show the utility of SchWARMA in a multi-qubit circuit simulation, as it results in substantial computational savings over a stochastic Liouville approach.

Example 1: Quantum Noise Spectroscopy—In this first example, we verify that the SchWARMA noise spectrum is consistent with quantum noise spectroscopy. The power spectrum $S_y(\omega)$ of the output y of an ARMA model driven by i.i.d. Gaussian noise is

$$S_y(\omega) = \frac{|\sum_{k=0}^q b_k \exp(-ik\omega)|^2}{|1 + \sum_{k=1}^p a_k \exp(-ik\omega)|^2}. \quad (8)$$

We model the dephasing dynamics of a qubit with the Hamiltonian $H(t) = \eta(t)\sigma_z + \Omega(t)\sigma_x$ using SchWARMA, where η is a stationary and Gaussian semi-classical noise and Ω infinitely fast control (as in a quantum circuit model). Dephasing noise leads to decay in the survival probability p of a qubit both prepared and measured in the $|+\rangle$ state (assuming no state preparation and measurement error), given by $p = 1/2[1 + \exp(-\int d\omega |F(\omega)|^2 S_y(\omega))]$ where $F(\omega)$ is the filter function (Fourier transform of the control's modulation function, for single axis X control) [46, 47]. Under these assumptions, the noise spectrum can be inferred by applying different control inputs. Here, we use different gate sequences to define a regression problem in the fashion of [48–50], details in [39]. Exploiting the universality of ARMA models in producing arbitrary power spectra, SchWARMA simulations of quantum noise spectroscopy for several spectra are shown in Fig. 1. The estimates produced are in strong agreement with

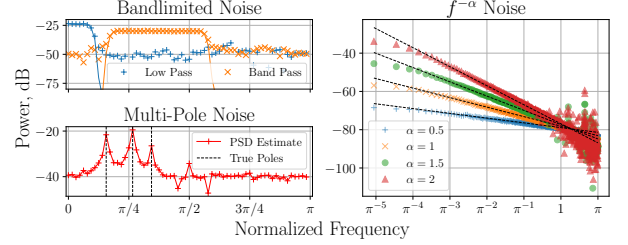


FIG. 1. Upper left: Spectrum reconstructions (markers) of SchWARMA simulated low-pass and band-pass noise (lines). Lower left: Spectrum reconstruction of SchWARMA simulated “peaky” multi-pole AR spectrum. Right: Spectrum reconstructions of SchWARMA simulated $f^{-\alpha}$ noise, dashed lines indicate ideal α .

the true spectra, with the primary limiting factors being Monte Carlo accuracy and conditioning of the system of equations.

Example 2: Dynamical Decoupling—Next, consider a single qubit in the presence of multi-axis noise and control,

$$H(t) = \sum_{i=\{x,y,z\}} \eta_i(t)\sigma_i + \Omega(t)(\cos(\phi)\sigma_x + \sin(\phi)\sigma_y), \quad (9)$$

where $\eta_i(t)$ are zero-mean wide-sense stationary Gaussian processes with correlation functions $\langle \eta_i(\tau)\eta_j(t) \rangle = f_i(|\tau - t|)\delta_{ij}$, ϕ is a user-controlled parameter that specifies the axis of rotation, and $\Omega(t)$ is the time-dependent amplitude of the control pulse. Furthermore, let the η_i have correlation functions $f_i(\tau) = \frac{\gamma_i}{2\sqrt{\pi}\tau_{c,i}} \exp\left(\frac{-\tau^2}{4\tau_{c,i}^2}\right)$, where $\tau_{c,i}$ is the correlation-time of the noise for axis i and γ_i is the corresponding noise-amplitude.

Decoupling control protocols can be an effective mechanism for reducing decoherence. The key to their error suppression ability is the fact that no error process happens instantaneously, despite this being a commonly made approximation in the theory of open quantum systems. If one can control the system on a time-scale fast relative to the error dynamics then error-suppression is possible with these protocols [51–54]. Furthermore, some protocols are more effective at suppressing different classes of noise compared to others. In particular, the $XY4$ protocol [55] suppresses multi-axis semi-classical errors to second order, whereas repeated XX gates only suppress Y and Z errors to second order. Fig. 2 (left) shows SchWARMA reproducing these phenomena in terms of process fidelity, using the Hamiltonian in Eq. 9 with separate ARMA models driving the η_i , and instantaneous π control pulses. The process fidelity $F_p(U, \Phi)$ at each time-step between the ideal unitary operator U , and the average noisy map, is defined as $(1/N^2)Tr[(U^\top \otimes U^\dagger)(\sum_k M_k^* \otimes M_k)]$, where $*$ and \top denote complex conjugation and transpose, respectively.

As discussed above, SchWARMA is also capable of simulating time-correlations with arbitrary CP-divisible errors, including non-unital channels; for e.g. amplitude damping. Here, decoupling protocols will not reduce decoherence as we assume an infinitely fast bath, but consider the *non-unital*

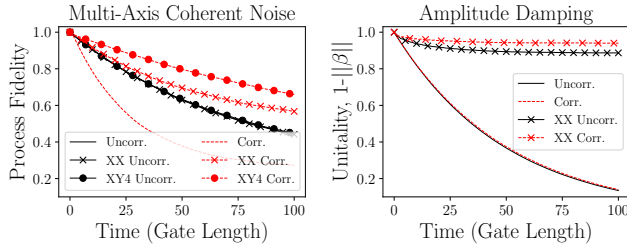


FIG. 2. Left: Process fidelity decay due to multi-axis coherent noise. Correlated noise ($\tau_c = 3$) produces more rapid decay than uncorrelated noise. Decoupling protocols reduce the decay for correlated case, with slower decay for $XY4$ than XX . Right: Decay in unitarity from amplitude damping. Uncontrolled decay is essentially identical, but decoupling protocols better preserve unitarity for correlated damping ($\tau_c = 3$). In this case, XX and $XY4$ (not shown) are identical.

action of the map. All CPTP maps have an affine form [56], visualized in Bloch space as a combination of a unital contraction and rotation operations along with a non-unital shift from the origin. This shift is defined by the vector β , $\beta_i = \langle\langle I_N | \sum M_k^* \otimes M_k | \sigma_i \rangle\rangle$, where $|\cdot\rangle\rangle$ denotes column stacking and $\langle\langle \cdot | = |\cdot\rangle\rangle^\dagger$. For amplitude damping β shifts the origin towards $|0\rangle$. However, decoupling sequences will flip the direction of this shift, resulting in slower rate of unitality ($1 - \|\beta\|$) decay, as depicted in Fig. 2 (right). This demonstrates SchWARMA can simulate the impact of temporally-correlated classical noise processes that affect the rate of decoherence even for non-unital channels such as those observed in [45].

Example 3: Quantum Circuit Simulation—Next, we simulate noisy multi-qubit quantum circuits with entangling two-qubit interactions, and multi-axis single-qubit dephasing noise [similar to Eq. (9)]. Thus, our model contains multi-axis temporally-correlated noise without any spatial-correlations. We assume a tunable interaction along $\sigma_z^{(k)} \otimes \sigma_z^{(j)}$ between qubits k and j , with strength $\Omega_{ZZ}^{(k,j)}(t)$.

We simulate the X and Z check circuits for the surface code [57]. The trajectories are also simulated using a full density-matrix simulation of the noisy pulse sequence using a first-order Trotter-Suzuki technique [40–43] and square pulse shapes, and compared to the SchWARMA model approximation for different noise amplitudes and correlation times. The SchWARMA simulation assumes the gates to be perfect and instantaneous and follows each gate with a random unitary rotation from the SchWARMA model: $S_k^{(j)} = \exp(-i \sum_{\mu=x,y,z} y_k^{(j,\mu)} \sigma_\mu^{(j)})$ for each qubit j at time-step k . We compile the circuits into our gate set to produce equivalent circuits with single-qubit X and Y controls and a two-qubit ZZ interaction. Single-qubit gate-times are normalized to unity, while the two-qubit gate-times are set to four times the single qubit gate-times. Further details are provided in the supplement [39].

We compare the process-infidelity $1 - F_p$ of Monte Carlo

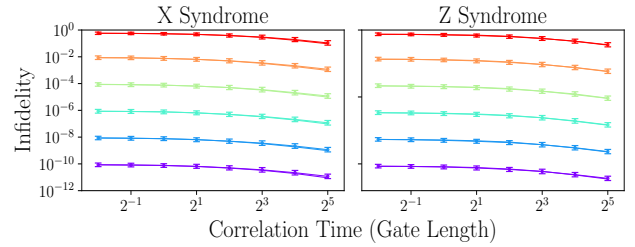


FIG. 3. Process infidelities for surface code X (left) and Z (right) check circuits as a function of noise parameters $\tau_{c,i}$ (x -axis) and γ_i (color) defined below Eq. (9). The noise strength is equal on each axis ($\gamma_x = \gamma_y = \gamma_z$) and qubit with $\gamma_i \in \{10^{-12}, 10^{-10}, \dots, 10^{-2}\}$ (bottom to top) in units of inverse gate length. The Trotter approach is plotted as a line while the SchWARMA simulation is plotted as marks along with Monte Carlo error bars.

averaged CPTP maps for a five qubit circuit in Fig. 3. The SchWARMA model (shown as points) shows very good agreement with the full trotter simulation (solid line). It takes about three orders of magnitude less computational time as we set our Trotter time step to be 0.001 single-qubit gate-lengths, while our SchWARMA model steps in units of gates within the circuit. This example highlights the utility of using SchWARMA to simulate correlated noise within quantum circuits, with a complexity no worse than a state-vector simulator such as the ones used in Refs. [58, 59].

Discussion and Future Work—We presented an approach, motivated by classic ARMA modeling techniques, that parameterizes and simulates time-correlated dynamics in quantum systems. To highlight the versatility of this technique, we demonstrated its applicability in simulating dephasing noise (single and multi-axis) and non-unital dissipative noise, applied to single qubits as well as multi-qubit circuits. It is straightforward to extend these techniques to simulate continuously driven systems such as adiabatic dynamics in multi-qubit and qutrit systems [39]. The single-qubit (and qutrit) simulations using SchWARMA produce strong agreement with established theory, and the multi-qubit simulations tracked accurately to stochastic Liouville simulations, at substantial computational savings.

The results presented here open up many avenues for future work. The ability to generate temporally-correlated errors at a low computational cost can be immediately applied to circuit simulations relevant to quantum error correction, such as for threshold analysis in the presence of absolutely continuous errors [59]. Similarly, SchWARMA could be used to analyze and extend techniques for quantum state, process, and gate-set tomography in the presence of correlated noise. Furthermore, they may be incorporated in tomographic algorithms designed to handle correlated noise as well as for parametric quantum noise spectroscopy. Given the connections between ARMA models and the fields of spectrum estimation, classical signal processing, and control, we believe there are a number of straightforward generalizations from the classical realm to

that of open quantum systems. In particular, this approach could be a “discrete time” analogue to the filter function formalism [47, 60].

Acknowledgments—We thank Colin Trout, Tim Sweeney, Lorenza Viola, and Leigh Norris for reviewing the manuscript and for fruitful conversations during its preparation. KS, GQ, and PT acknowledge funding from the DOE Office Science contract 4000167418. KS, GQ, PT, and BDC acknowledge funding from the DOE Office of Science Grant Number DE-SC0020316. KS and GQ acknowledge support from ARO MURI grant W911NF-18-1-0218. A portion of this research was supported by the Intelligence Advanced Research Projects Activity via Department of Interior National Business Center contract number 2012- 12050800010. The U.S. Government is authorized to reproduce and distribute reprints for Governmental purposes notwithstanding any copyright annotation thereon. The views and conclusions contained herein are those of the authors and should not be interpreted as necessarily representing the official policies or endorsements, either expressed or implied, of IARPA, DoI/NBC, or the U.S. Government.

-
- [1] D. Deutsch, *Proceedings of the Royal Society of London. A. Mathematical and Physical Sciences* **400**, 97 (1985).
- [2] A. Chi-Chih Yao, in *Proceedings of 1993 IEEE 34th Annual Foundations of Computer Science* (1993) pp. 352–361.
- [3] M. A. Nielsen and I. L. Chuang, *Quantum computation and quantum information* (Cambridge university press, 2010).
- [4] D. Deutsch and R. Jozsa, *Proceedings of the Royal Society of London. Series A: Mathematical and Physical Sciences* **439**, 553 (1992).
- [5] L. K. Grover, in *Proceedings of the Twenty-eighth Annual ACM Symposium on Theory of Computing*, STOC ’96 (ACM, New York, NY, USA, 1996) pp. 212–219.
- [6] P. W. Shor, *SIAM Journal on Computing* **26**, 1484 (1997), <https://doi.org/10.1137/S0097539795293172>.
- [7] P. W. Shor, in *Proceedings of 37th Conference on Foundations of Computer Science* (1996) pp. 56–65.
- [8] D. Aharonov and M. Ben-Or, in *Proceedings of the Twenty-ninth Annual ACM Symposium on Theory of Computing*, STOC ’97 (ACM, New York, NY, USA, 1997) pp. 176–188.
- [9] D. Gottesman, *Phys. Rev. A* **57**, 127 (1998).
- [10] R. C. Bialczak, R. McDermott, M. Ansmann, M. Hofheinz, N. Katz, E. Lucero, M. Neeley, A. D. O’Connell, H. Wang, A. N. Cleland, and J. M. Martinis, *Phys. Rev. Lett.* **99**, 187006 (2007).
- [11] J. Bylander, S. Gustavsson, F. Yan, F. Yoshihara, K. Harrabi, G. Fitch, D. G. Cory, Y. Nakamura, J.-S. Tsai, and W. D. Oliver, *Nature Physics* **7**, 565 (2011).
- [12] J. Burnett, L. Faoro, I. Wisby, V. L. Gurtovoi, A. V. Chernykh, G. M. Mikhailov, V. A. Tulin, R. Shaikhaidarov, V. Antonov, P. J. Meeson, A. Y. Tzalenchuk, and T. Lindström, *Nature Communications* **5**, 4119 (2014).
- [13] P. Kumar, S. Sendelbach, M. A. Beck, J. W. Freeland, Z. Wang, H. Wang, C. C. Yu, R. Q. Wu, D. P. Pappas, and R. McDermott, *Phys. Rev. Applied* **6**, 041001 (2016).
- [14] J. J. Burnett, A. Bengtsson, M. Scigliuzzo, D. Nipece, M. Ku- dra, P. Delsing, and J. Bylander, *npj Quantum Information* **5**, 54 (2019).
- [15] G. A. Álvarez and D. Suter, *Phys. Rev. Lett.* **107**, 230501 (2011).
- [16] K. Willick, D. K. Park, and J. Baugh, *Phys. Rev. A* **98**, 013414 (2018).
- [17] Y. Romach, C. Müller, T. Unden, L. J. Rogers, T. Isoda, K. M. Itoh, M. Markham, A. Stacey, J. Meijer, S. Pezzagna, B. Naydenov, L. P. McGuinness, N. Bar-Gill, and F. Jelezko, *Phys. Rev. Lett.* **114**, 017601 (2015).
- [18] F. Yan, D. Campbell, P. Krantz, M. Kjaergaard, D. Kim, J. L. Yoder, D. Hover, A. Sears, A. J. Kerman, T. P. Orlando, S. Gustavsson, and W. D. Oliver, *Phys. Rev. Lett.* **120**, 260504 (2018).
- [19] K. W. Chan, W. Huang, C. H. Yang, J. C. C. Hwang, B. Hensen, T. Tanttu, F. E. Hudson, K. M. Itoh, A. Laucht, A. Morello, and A. S. Dzurak, *Phys. Rev. Applied* **10**, 044017 (2018).
- [20] V. M. Frey, S. Mavadia, L. M. Norris, W. de Ferranti, D. Lucarelli, L. Viola, and M. J. Biercuk, *Nature Communications* **8**, 2189 (2017).
- [21] R. Kubo, *Journal of Mathematical Physics* **4**, 174 (1963).
- [22] P. Whittle, *Prediction and regulation by linear least-square methods* (English Universities Press, 1963).
- [23] G. E. Box, G. M. Jenkins, G. C. Reinsel, and G. M. Ljung, *Time series analysis: forecasting and control* (John Wiley & Sons, 2015).
- [24] S. M. Kay and S. L. Marple Jr, *Proceedings of the IEEE* **69**, 1380 (1981).
- [25] H.-P. Breuer and F. Petruccione, *The theory of open quantum systems* (Oxford University Press on Demand, 2002).
- [26] A. Rivas, S. F. Huelga, and M. B. Plenio, *Reports on Progress in Physics* **77**, 094001 (2014).
- [27] E. Knill, D. Leibfried, R. Reichle, J. Britton, R. B. Blakestad, J. D. Jost, C. Langer, R. Ozeri, S. Seidelin, and D. J. Wineland, *Phys. Rev. A* **77**, 012307 (2008).
- [28] R. Blume-Kohout, J. King Gamble, E. Nielsen, J. Mizrahi, J. D. Sterk, and P. Maunz, arXiv e-prints , arXiv:1310.4492 (2013), arXiv:1310.4492 [quant-ph].
- [29] S. T. Merkel, J. M. Gambetta, J. A. Smolin, S. Poletto, A. D. Córcoles, B. R. Johnson, C. A. Ryan, and M. Steffen, *Phys. Rev. A* **87**, 062119 (2013).
- [30] D. Greenbaum, arXiv e-prints , arXiv:1509.02921 (2015), arXiv:1509.02921 [quant-ph].
- [31] J. Cerrillo and J. Cao, *Phys. Rev. Lett.* **112**, 110401 (2014).
- [32] S. H. Holan, R. Lund, G. Davis, *et al.*, *Statistics Surveys* **4**, 232 (2010).
- [33] A. R. Ives, K. C. Abbott, and N. L. Ziebarth, *Ecology* **91**, 858 (2010).
- [34] E. W. Frees, Y.-C. Kung, M. A. Rosenberg, V. R. Young, and S.-W. Lai, *North American Actuarial Journal* **1**, 49 (1997).
- [35] I. M. James, *The topology of Stiefel manifolds*, Vol. 24 (Cambridge University Press, 1976).
- [36] S. Fiori, *Circuits, Systems, and Signal Processing* **33**, 2449 (2014).
- [37] M.-D. Choi, *Linear Algebra and its Applications* **10**, 285 (1975).
- [38] A. Edelman, T. A. Arias, and S. T. Smith, *SIAM journal on Matrix Analysis and Applications* **20**, 303 (1998).
- [39] See Supplemental Material for additional details.
- [40] M. Suzuki, *Communications in Mathematical Physics* **51**, 183 (1976).
- [41] M. Suzuki, *Communications in Mathematical Physics* **57**, 193 (1977).
- [42] M. Suzuki, *Journal of Mathematical Physics* **26**, 601 (1985).
- [43] M. Suzuki, *Physics Letters A* **146**, 319 (1990).

- [44] D. W. Berry, G. Ahokas, R. Cleve, and B. C. Sanders, *Communications in Mathematical Physics* **270**, 359 (2007).
- [45] P. V. Klimov, J. Kelly, Z. Chen, M. Neeley, A. Megrant, B. Burkett, R. Barends, K. Arya, B. Chiaro, Y. Chen, A. Dunsworth, A. Fowler, B. Foxen, C. Gidney, M. Giustina, R. Graff, T. Huang, E. Jeffrey, E. Lucero, J. Y. Mutus, O. Naaman, C. Neill, C. Quintana, P. Roushan, D. Sank, A. Vainsencher, J. Wenner, T. C. White, S. Boixo, R. Babbush, V. N. Smelyanskiy, H. Neven, and J. M. Martinis, *Phys. Rev. Lett.* **121**, 090502 (2018).
- [46] L. Cywiński, R. M. Lutchyn, C. P. Nave, and S. Das Sarma, *Phys. Rev. B* **77**, 174509 (2008).
- [47] G. A. Paz-Silva and L. Viola, *Phys. Rev. Lett.* **113**, 250501 (2014).
- [48] G. A. Álvarez and D. Suter, *Phys. Rev. Lett.* **107**, 230501 (2011).
- [49] P. Szańskiowski, G. Ramon, J. Krzywda, D. Kwiatkowski, and Ł. Cywiński, *Journal of Physics: Condensed Matter* **29**, 333001 (2017).
- [50] G. A. Paz-Silva, L. M. Norris, and L. Viola, *Phys. Rev. A* **95**, 022121 (2017).
- [51] L. Viola and S. Lloyd, *Phys. Rev. A* **58**, 2733 (1998).
- [52] L. Viola, E. Knill, and S. Lloyd, *Phys. Rev. Lett.* **82**, 2417 (1999).
- [53] P. Zanardi, *Physics Letters A* **258**, 77 (1999).
- [54] M. Byrd and D. Lidar, *Quant. Info. Proc.* **1**, 19 (2002).
- [55] A. Maudsley, *Journal of Magnetic Resonance* (1969) **69**, 488 (1986).
- [56] A. Fujiwara and P. Algoet, *Phys. Rev. A* **59**, 3290 (1999).
- [57] A. G. Fowler, M. Mariantoni, J. M. Martinis, and A. N. Cleland, *Phys. Rev. A* **86**, 032324 (2012).
- [58] Y. Tomita and K. M. Svore, *Phys. Rev. A* **90**, 062320 (2014).
- [59] J. P. Barnes, C. J. Trout, D. Lucarelli, and B. D. Clader, *Phys. Rev. A* **95**, 062338 (2017).
- [60] A. G. Kofman and G. Kurizki, *Phys. Rev. Lett.* **87**, 270405 (2001).

Supplemental Material for “SchWARMA: A model-based approach for time-correlated noise in quantum circuits”

This supplement is divided in several sections expanding on the results in the main text, providing additional details of the theory, simulations, practical considerations, and further examples. The first section, Sec. S.I derives the relationship between SchWARMA steps on Stiefel manifolds and the Lindblad master equation, showing a correspondence between the Stiefel manifold tangent vectors and traditional Hamiltonian and Lindblad generators. In Sec. S.II, we provide a brief overview of ways to tailor the underlying ARMA model coefficients to generate noise of a desired spectra as well as “normalizing” noise models between time scales. The next section, Sec. S.III provides additional details and discussion about the SchWARMA models used in the main text. The next two sections, Secs. S.IV and S.V provide further details about the quantum noise spectroscopy simulations and surface code circuit simulation, respectively. Finally, in Sec. S.VI, we introduce a fundamentally different usage of SchWARMA to model noise in continuously driven (as opposed to gate-based) quantum systems. Source code for examples and figures in the main text and supplement can be found at [S1].

S.I. RELATIONSHIP BETWEEN SCHWARMA AND LINDBLAD MASTER EQUATION

The Lindblad master equation [S2–S4] can be viewed as a differential version of a CPTP map under Markovian evolution. In this section we will show the relationship between the Lindblad master equation and dynamics on Stiefel manifolds and thus the SchWARMA approach. A convenient form of the Lindblad master equation is

$$\dot{\rho} = -i[H, \rho] + \sum_{\alpha} \left(L_{\alpha} \rho L_{\alpha}^{\dagger} - \frac{1}{2} \{ L_{\alpha}^{\dagger} L_{\alpha}, \rho \} \right) \quad (\text{S1})$$

where H is the system Hamiltonian, and $\{L_{\alpha}\}$ are the so-called Lindblad operators. We will essentially follow the derivation in [S5] using the stacked Kraus operator formulation of SchWARMA. In particular, we show that the tangent space elements of the Stiefel manifold are related to the Lindblad generators.

Consider an arbitrary Stiefel manifold tangent space element decomposed into $N \times N$ blocks

$$X = \begin{bmatrix} A \\ B_1 \\ \vdots \\ B_{K-1} \end{bmatrix} \quad (\text{S2})$$

recalling that A is skew symmetric like the matrix $-iH$ for an arbitrary Hamiltonian. The SchWARMA approach utilizes the exponential map on the Stiefel manifold, which corresponds to a $KN \times KN$ unitary evolution of a density matrix consisting of the system and the environment, in the spirit of the

Stinespring form of the CPTP map [S6]. This is then followed by tracing out the environment to obtain the evolution of the system density matrix.

Let us start by showing, how an individual SchWARMA step relates to the evolution of density matrices under CPTP maps. The propagation of a joint system-environment state ρ_{ES} is given by joint unitary dynamics,

$$\dot{\rho}_{ES} = \left[\begin{pmatrix} A & -B^{\dagger} \\ B & \mathbf{0} \end{pmatrix}, \rho_{ES} \right] \triangleq [iH_{ES}, \rho_{ES}] \quad (\text{S3})$$

where, the initial state of the system+environment is considered to be unentangled, $\rho_{ES}(0) = |0_E\rangle\langle 0_E| \otimes \rho_S(0)$ and $B = [B_1^{\dagger}, \dots, B_{K-1}^{\dagger}]^{\dagger}$. For a SchWARMA gate time T , and constant A and B , this results in $\rho_{ES}(T) = U_{ES}(T)\rho_{ES}(0)U_{ES}(T)^{\dagger}$ where

$$U_{ES}(T) = \exp \left(T \begin{bmatrix} A & -B^{\dagger} \\ B & \mathbf{0} \end{bmatrix} \right). \quad (\text{S4})$$

The second piece of an individual SchWARMA step is to trace out the environment, so that $\rho_S(T) = \text{Tr}_E(\rho_{ES}(T))$ which amounts to Kraus operators

$$\rho_S(T) = \sum_{k=1}^K M_k(T) \rho_S(0) M_k(T)^{\dagger} \quad (\text{S5})$$

where

$$M_k(T) = (\langle k_E | \otimes I_N) U_{ES}(T) I_{KN^2, N}, \quad (\text{S6})$$

where I_N is the $N \times N$ identity matrix and $I_{KN^2, N}$ is the first N columns of I_{KN^2} . In other words, the Kraus operators are the $N \times N$ blocks of the first N columns of U_{ES} , as desired.

Next, we will analyze these dynamics in the limit of small T to show how they relate to the Lindblad master equation. For small ΔT , we could say that

$$U_{ES}(\Delta T) \approx I_{ES} + \Delta T \begin{bmatrix} A & -B_1^{\dagger} & \dots \\ B_1 & \mathbf{0} & \\ \vdots & & \end{bmatrix}, \quad (\text{S7})$$

to determine the limiting Kraus operators $M_k(\Delta T)$. However, this ignores the Stiefel manifold orthonormal column constraint (equivalently, the TP constraint) so we need some correction B_0 where

$$(I_N + A + B_0)^{\dagger} (I_N + A + B_0) = I_N - \sum_{k=1}^{K-1} B_k^{\dagger} B_k, \quad (\text{S8})$$

so

$$A^{\dagger} + A + B_0^{\dagger} + B_0 + \mathcal{O}(\Delta T^2) = - \sum_{k=1}^{K-1} B_k^{\dagger} B_k. \quad (\text{S9})$$

note that A is skew-Hermitian (so $A^\dagger + A = 0$) and thus

$$B_0 = -\frac{1}{2} \sum_{k=1}^{K-1} B_k^\dagger B_k. \quad (\text{S10})$$

This suggests a set of infinitesimal Kraus operators

$$M_k(\Delta T) \approx \begin{cases} I_N + A + B_0, & k = 1 \\ B_{k-1}, & 2 \leq k \leq K. \end{cases} \quad (\text{S11})$$

Then, in a similar fashion to [S5], our Stiefel manifold construction has (up to order ΔT)

$$\rho + \Delta\rho = (I + A + B_0)\rho(I + A + B_0)^\dagger + \sum_{k=1}^{K-1} B_k \rho B_k^\dagger. \quad (\text{S12})$$

Subtracting ρ from both sides and substituting $A = -iH$, we have

$$\Delta\rho = -i[H, \rho] + \{B_0, \rho\} + (A + B_0)\rho(A + B_0)^\dagger + \sum_{k=1}^{K-1} B_k \rho B_k^\dagger. \quad (\text{S13})$$

Note that the term $(A + B_0)\rho(A + B_0)^\dagger$ is second order in A and fourth order in B_i , so we have that, up to the original

order,

$$\Delta\rho = -i[H, \rho] + \{B_0, \rho\} + \sum_k^K B_k \rho B_k^\dagger \quad (\text{S14})$$

$$= -i[H, \rho] + \sum_{k=1}^K \left(B_k \rho B_k^\dagger - \frac{1}{2} \{B_k^\dagger B_k, \rho\} \right). \quad (\text{S15})$$

This indicates several relevant factors for SchWARMA. First, to identify tangent space elements that generate target non-unitary Kraus operators (with some parametric form), we need to first find the Kraus operator that can be set closest to I_N , then set B_k to the Kraus operators that are not that near- I_N operator. Equivalently, if we have a known master equation in the above canonical form that we wish to emulate with SchWARMA, the Stiefel manifold tangent elements B_k should be set to L_α . Again, while the Lindblad and SchWARMA approaches are equivalent to first order, SchWARMA temporarily propagates the bath and so the trajectories will diverge. That said, it is clear that small SchWARMA steps will approximate the Lindblad master equation. Furthermore, as the SchWARMA approach as formulated always produces CPTP maps (that may arise from non-CP divisible trajectories), a CP-divisible trajectory could be derived from the Lindblad master equation that produces equivalent maps at the gate time-scale.

This suggests an alternative (and essentially equivalent) usage of SchWARMA for stochastic Lindblad master equations where individual time-correlated steps are defined by

$$|\rho_{k+1}\rangle\rangle = \exp \left(-iI_N \otimes H_k - iH_k \otimes I_N + \sum_\alpha \|\mathbf{y}_k^{(\alpha)}\|^2 \left(L_\alpha^* \otimes L_\alpha - \frac{1}{2} I \otimes L_\alpha^\dagger L_\alpha - \frac{1}{2} (L_\alpha^\dagger L_\alpha)^\top \otimes I \right) \right) |\rho_k\rangle\rangle, \quad (\text{S16})$$

where H_k is a "unitary" SchWARMA Hamiltonian, and $\mathbf{y}_k^{(\alpha)}$ are the outputs of (possibly complex) ARMA models as in the original SchWARMA formulation. This formulation is clearly dissipative and CP-divisible, as the coefficients Lindblad coefficient $\|\mathbf{y}_k^{(\alpha)}\|^2$ are nonnegative. It is clear, however, that maintaining the SchWARMA "bath" offers a potential path forward for non-CP divisible dynamics.

S.II. DETERMINING SCHWARMA MODEL COEFFICIENTS

The power spectrum of the noise generated by a SchWARMA model is determined by the underlying ARMA model coefficients. Furthermore, ARMA models are dense in the space of valid power spectra, allowing for SchWARMA approximations of any power spectra. Digital signal processing has a number of methods for determining ARMA coefficients, referred to in this domain as *filter design*. Band-limited (including low-pass, band-pass, high-pass, and multi-band)

spectra can be parametrically generated using window-based methods, with the choice of window determining features such as flatness in the pass-bands, roll-off rate to stop-bands, and overall suppression in the stop-bands [S7]. Other options for filter design can produce (approximate) fits for arbitrary given spectra, such as the Parks-McClellan algorithm [S8] or convex optimization [S9]. Specific techniques exist for certain spectra, such as $f^{-\alpha}$ noise [S10] or line spectra [S11, Ch. 4].

In this work, we are also faced with the challenge of taking a parametrically defined noise spectrum at a fine time scale (the Trotter "step" of our stochastic master equation) and computing an equivalent effective noise at a coarser time scale (the "gate" time scale of SchWARMA). We assume that both noises are Gaussian and wide-sense stationary with discrete-time autocovariance functions $r_f[k]$ and $r_s[k]$ for the "fast" master equation time scale and the "slow" SchWARMA time scale, respectively. Supposing we wish to design a SchWARMA model that effectively captures the noise at an integer factor T slower, it is not sufficient to set $r_s[k] = r_f[kT]$, as this ignores the intuition that the fast noise should

be in some sense integrated (i.e., added) during the T steps of the faster model, as in a random walk. Thus, we need to relate $r_s[k]$ to the sum of T steps of the fast model. To achieve this, we exploit the well-known relationship about the variance of

the sum of correlated Gaussians X_i :

$$\text{Var} \left(\sum_{i=1}^N X_i \right) = \sum_{i=1}^N \text{Var}(X_i) + 2 \sum_{1 \leq i < j \leq N} \text{Cov}(X_i, X_j). \quad (\text{S17})$$

Given a target fast time scale noise autocovariance r_f we can set up a system of P equations to solve for the unknown r_s using

$$r_s[0] = Tr_f[0] + 2 \sum_{i=1}^{T-1} (T-i)r_f[i], \quad (\text{S18})$$

$$2r_s[0] + 2r_s[1] = 2Tr_f[0] + 2 \sum_{i=1}^{2T-1} (2T-i)r_f[i], \quad (\text{S19})$$

\vdots P times

$$Pr_s[0] + 2 \sum_{j=1}^{P-1} (P-j)r_s[j] = PTr_f[0] + 2 \sum_{i=1}^{PT-1} (PT-i)r_f[i], \quad (\text{S20})$$

where we have substituted e.g., $r_f[|i-j|]$ for $\text{Cov}(X_i, X_j)$ per the definition of wide sense stationary. Note that the left hand side of the equations correspond to the variance of the sum of the slow time process, and the right hand side is the variance of the sum of the fast time process sampled every T steps. Next, we then use the spectral factorization approach to filter design outlined in [S9] to generate coefficients for a SchWARMA model.

S.III. SCHWARMA MODELS FOR QUANTUM NOISE SPECTROSCOPY AND SURFACE CODES

Here we provide details of how we implement the SchWARMA models for our various examples. As a reminder, the SchWARMA model is given by (c.f. Eq. (4) in main text):

$$y_k^{(\ell)} = \sum_{i=1}^p a_i^{(\ell)} y_{k-i}^{(\ell)} + \sum_{j=0} b_j^{(\ell)} x_{k-j}^{(\ell)} \quad (\text{S21a})$$

$$\mathcal{S}_k = \exp_{\mathcal{U}_k} \left(\sum_{\ell=1}^L y_k^{(\ell)} X^{(\ell)} \right), \quad (\text{S21b})$$

where

$$\exp_{\mathcal{U}_k} \left(\begin{bmatrix} A \\ B \end{bmatrix} \right) = \begin{bmatrix} U & \mathbf{0} \\ \mathbf{0} & I_{KN-N} \end{bmatrix} \exp \left(\begin{bmatrix} A & -B^\dagger \\ B & \mathbf{0} \end{bmatrix} \right) I_{KN,N}, \quad (\text{S22})$$

for ideal unitary U , its corresponding stiefel representation \mathcal{U}_k , and tangent space element

$$X = \begin{bmatrix} A \\ B \end{bmatrix}, \quad (\text{S23})$$

with A an $N \times N$ skew-symmetric complex matrix, and B an $KN \times N$ arbitrary complex matrix.

Consider an example where we wish to simulate correlated noise within a quantum circuit such as the one shown schematically in Fig. S1 for arbitrary one and two qubit gates specified as G_i . For the noise model, we create two SchWARMA models (denoted by an additional upper index on \mathcal{S}_k) given by Eq. (S21b) with $U = I_2$ chosen to be the identity as we want to sample our error channel near the identity. This allows one to simply insert random noise channels into the circuit with the amplitude of the noise determined by the ARMA coefficients given in Eq. (S21a). Specific choices of noise channel are considered next.

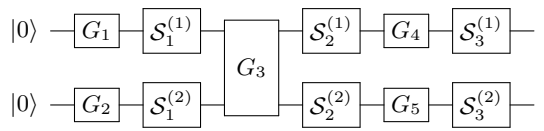


FIG. S1. Circuit schematic demonstrating how one might implement a SchWARMA model within a circuit of arbitrary one and two qubit gates labelled with G_i . It allows one to consider perfect gates followed by noise that retains the time correlation. The $S_k^{(q)}$ terms are the error channel defined in Eq. (S21b) with additional upper index denoting the qubit.

A. Z Dephasing

We define a Z dephasing SchWARMA model with:

$$U = \begin{bmatrix} 1 & 0 \\ 0 & 1 \end{bmatrix}, \quad (\text{S24a})$$

$$X = -i\sigma_z = \begin{bmatrix} -i & 0 \\ 0 & i \end{bmatrix}, \quad (\text{S24b})$$

so $N = 2$ and $K = 1$, corresponding to unitary dynamics on a qubit. Since $K = 1$, we have that $\exp_{\mathcal{U}_k}$ is the usual matrix exponential and this gives the map to apply at circuit location k by the simple expression

$$\mathcal{S}_k = \begin{bmatrix} e^{-iy_k} & 0 \\ 0 & e^{iy_k} \end{bmatrix}, \quad (\text{S25})$$

where we have suppressed the ℓ index, since there is only a single SchWARMA model needed. This is nothing more than a Z rotation by an angle given by a classical ARMA model.

B. Multi-axis Dephasing

For the slightly more complication multi-axis noise that we consider for our surface code simulations, the SchWARMA model is given by:

$$U = \begin{bmatrix} 1 & 0 \\ 0 & 1 \end{bmatrix}, \quad (\text{S26a})$$

$$X^{(x)} = -i\sigma_x = \begin{bmatrix} 0 & -i \\ -i & 0 \end{bmatrix}, \quad (\text{S26b})$$

$$X^{(y)} = -i\sigma_y = \begin{bmatrix} 0 & -1 \\ 1 & 0 \end{bmatrix}, \quad (\text{S26c})$$

$$X^{(z)} = -i\sigma_z = \begin{bmatrix} -i & 0 \\ 0 & i \end{bmatrix}, \quad (\text{S26d})$$

so, again, $N = 2$ and $K = 1$, corresponding to unitary dynamics, but this time with $L = 3$ corresponding to multiple underlying ARMA models. Again, we have that $\exp_{\mathcal{U}_k}$ is the usual matrix exponential for qubit unitary dynamics, and this gives the map to apply at circuit location k by the expression

$$\mathcal{S}_k = \exp[-i(y_k^{(x)}\sigma_x + y_k^{(y)}\sigma_y + y_k^{(z)}\sigma_z)] \quad (\text{S27})$$

$$= \begin{bmatrix} \cos(g_k) - iy_k^{(z)}\text{sinc}(g_k) & -(iy_k^{(x)} - y_k^{(y)})\text{sinc}(g_k) \\ -(iy_k^{(x)} + y_k^{(y)})\text{sinc}(g_k) & \cos(g_k) + iy_k^{(z)}\text{sinc}(g_k) \end{bmatrix}, \quad (\text{S28})$$

where $g_k = \sqrt{y_k^{(x)^2} + y_k^{(y)^2} + y_k^{(z)^2}}$, $N = 1$, and $\text{sinc}(x) = \sin(x)/x$.

C. Amplitude Damping

Finally, we consider the SchWARMA model for the non-unitary amplitude damping channel that we consider

within the main text. The tangent space element for that SchWARMA model is :

$$X = \begin{bmatrix} \mathbf{0}_{2 \times 2} & 0 & 0 \\ 0 & 1 & 0 \\ 0 & 0 & \mathbf{0}_{2 \times 2} \end{bmatrix} \quad (\text{S29})$$

where the notation $\mathbf{0}_{m \times n}$ indicates a matrix of zeros with m rows and n columns, $N = 2$, and $K = 2$. Thus S_k is given by:

$$S_k = \exp \left(y_k \begin{bmatrix} \mathbf{0}_{2 \times 2} & 0 & 0 \\ 0 & -1 & 0 \\ 0 & 1 & \mathbf{0}_{2 \times 2} \end{bmatrix} \right) I_{4,2}, \quad (\text{S30})$$

yielding an 4×2 sized matrix containing the two 2×2 Kraus operators. Since the tangent space element X in (S29) has all zeros in the skew-symmetric A component, in this case the driving ARMA model y_k can actually be complex-valued. These two Kraus operators at SchWARMA index k are:

$$M_1^{(k)} = \begin{bmatrix} 1 & 0 \\ 0 & \cos(|y_k|) \end{bmatrix}, \quad (\text{S31a})$$

$$M_2^{(k)} = \begin{bmatrix} 0 & \sin(|y_k|)e^{i\angle y_k} \\ 0 & 0 \end{bmatrix}. \quad (\text{S31b})$$

We see that this SchWARMA model is nothing more than the standard amplitude damping model, but with a decay coefficient given by the square of the sin of the absolute value of the classical ARMA model coefficient. We note that this process allows for some quantum processes that appear to be non-physical with, for example, negative amplitude damping coefficients. All channels created using this method are CPTP and physical. Since manifolds are only locally linear, when one takes a large step in the tangent space, the curvature of the manifold is not respected. Therefore, a direction that appears to be amplitude damping at the start of the curve will appear like something else relative to some point further along the curve defined by the arc.

Therefore, for $|y_k| < \pi/2$ we have classic amplitude damping, which includes both the non-unital shift towards $|0\rangle$ as well as anisotropic contractions in the X , Y , and Z dimensions of the Bloch sphere to maintain physicality. For $y_k = \pm\pi/2$ all states get mapped to the $|0\rangle$ state. For y_k between $\pi/2$ and π , the non-unital shift shrinks back to the origin and the contraction process reverses, except that the X and Y axes are both flipped. At $y_k = \pi$ we obtain the Z gate. This sequence is then reversed for $\pi < y_k < 2\pi$. The primary point here is that for non-unitary channels such as the amplitude damping channel, the step size should be small enough such that $0 \leq |y_k| < \pi/2$. For high-fidelity quantum operations, this will never be a concern.

D. Lindbladian Dephasing and Depolarizing

When averaged over random instances, the stochastic unitary SchWARMA models in sections S.III A and S.III B above

will produce, at each time step k , dephasing channels

$$\rho \rightarrow (1 - p_z)\rho + p_z\sigma_z\rho\sigma_z^\dagger \quad (\text{S32})$$

and depolarizing channels

$$\rho \rightarrow (1 - p_x - p_y - p_z)\rho + \sum_{j=x,y,z} p_j\sigma_j\rho\sigma_j^\dagger, \quad (\text{S33})$$

respectively, where the p_j are determined by the statistics of the underlying ARMA models at step k . At the SchWARMA level, this is fundamentally different from Lindblad style decay into an infinitely fast bath using Lindblad operators as described in S.I (i.e., $B_k \neq 0$). This is evident, for example, in the fact that SchWARMA errors corresponding to stochastic unitary evolution offer the potential of control (for time-correlated errors), whereas SchWARMA errors motivated by Lindblad evolutions will be purely dissipative regardless of the spectrum of the driving SchWARMA model. Furthermore, the correspondence between SchWARMA tangent vectors and the Lindblad master equation tells us that these Lindbladian-style depolarizing channels can be simulated in SchWARMA by $U = I_2$ and

$$X^{(x)} = \begin{bmatrix} \mathbf{0}_{2 \times 2} \\ \sigma_x \\ \mathbf{0}_{4 \times 2} \end{bmatrix}, \quad (\text{S34a})$$

$$X^{(y)} = \begin{bmatrix} \mathbf{0}_{4 \times 2} \\ \sigma_y \\ \mathbf{0}_{2 \times 2} \end{bmatrix}, \quad (\text{S34b})$$

$$X^{(z)} = \begin{bmatrix} \mathbf{0}_{6 \times 2} \\ \sigma_z \end{bmatrix}, \quad (\text{S34c})$$

with corresponding (possibly complex-valued) ARMA outputs $y_k^{(j)}$ for $j = x, y, z$. This model results in SchWARMA steps

$$\mathcal{S}_k = \exp\left(X_k^{(ES)}\right) I_{8,2}, \quad (\text{S35})$$

where

$$X_k^{(ES)} = \begin{bmatrix} \mathbf{0}_{2 \times 2} & -(y_k^{(x)}\sigma_x)^\dagger & -(y_k^{(y)}\sigma_y)^\dagger & -(y_k^{(z)}\sigma_z)^\dagger \\ y_k^{(x)}\sigma_x & & & \\ y_k^{(y)}\sigma_y & & & \\ y_k^{(z)}\sigma_z & & & \mathbf{0}_{6 \times 6} \end{bmatrix} \quad (\text{S36})$$

(c.f., Eq. S4) and the resulting error can be verified numerically to be four Kraus operators corresponding to a depolarizing channel. Clearly, the x and y terms can be dropped off and the z element “compacted” to a 4×2 matrix to restrict the errors to dephasing.

E. Additional SchWARMA Models

We emphasize that SchWARMA is not limited to the dephasing and amplitude damping cases considered above, or

even to channels near the identity as our examples have done. In particular, semi-classical noisy Hamiltonian dynamics are converted to SchWARMA models by multiplying the Hamiltonian elements by i , c.f., the single- and multi-axis dephasing examples above. The multiplication by i converts the Hermitian Hamiltonians to the skew-symmetric constraint needed for that portion of the Stiefel manifolds tangent space. This applies to arbitrary N -level systems including multi-qubit entangling noise. To extend the approach to arbitrary stochastic noise on Kraus operators, the log map for the Stiefel manifold [S12] can be used. Here, this corresponds to the standard matrix logarithm on the Kraus-stacked Stinespring form to compute its corresponding Lie algebra element (multiplied by i), where the first N columns correspond to the tangent space of the corresponding Stiefel manifold. This tangent space element can then be plugged in to Eq. (S21b) and driven by an ARMA model to produce correlated errors that correspond to the desired (non-unitary) error. We note that the log map can be numerically unstable so one should check that the exponentiation of the tangent space element corresponds to the desired map. In the rare cases we have encountered, these discrepancies are resolved using a bit of mathematical intuition to find the correct tangent space element from the matrix logarithm.

Beyond the application of SchWARMA general CPTP maps and arbitrary stationary Gaussian noise, the underlying ARMA formalism itself can be further generalized to model additional phenomena. At its core, SchWARMA is itself a non-linear vector ARMA (VARMA) model [S13, S14], and generalizing the underlying VARMA model can be done in a similar fashion to standard ARMA models, which would then scale the the tangent space elements and be matrix exponentiated. There is a rich field of generalizations of ARMA models in the literature [S14], which may be appropriate for different physical phenomenon than standard ARMA models. For example, ARIMA models nonstationary noise, SARMA and PARMA models are often used to model stochastic variations around some otherwise periodic behaviors, and GARCH models model volatility in the overall noise power [S15]. Additional nonlinearities could be used to model non-Gaussian semiclassical noise, such as that found in [S16]. We also expect that time-varying model coefficients and cross-correlated driving terms $x_k^{(\ell)}$ will find use in the modeling of control noise and spatial correlations, respectively.

S.IV. QUANTUM NOISE SPECTROSCOPY PROCESS

The noise generation was handled using Z -dephasing SchWARMA models. The bandlimited signals were MA models defined by a 128-tap Hamming window of desired bandwidth and cosine modulated to the appropriate center frequency (as needed). The multipole noise was generated by a purely AR SchWARMA model with coefficients set by placing three complex poles of the transfer function on the unit circle at locations corresponding to the desired peaks in the normalized frequency space and their complex conjugates. SchWARMA coefficients for the $f^{-\alpha}$ noise were generated using the methods in [S10].

To perform effective quantum noise spectroscopy, it is necessary to have spectrally diverse (in terms of the filter function) control sequences. To generate these, we used W different sequences of common length W gates (128 for the bandlimited and multipole noise, 2048 for the $f^{-\alpha}$ noise) whose discrete-time modulation functions [S17, S18] were defined by $f_k(m) = \text{sign}(\cos(\pi(k-1)m/W))$ for $k, m = 1, \dots, W$, meaning that an X gate is applied when the sign of the modulation function changed, or an I gate otherwise. Assuming ideal state preparation and measurement in $|+\rangle$, the Fourier transform of $f_k(m)$, $F_k(\omega)$, can be used to define a system of equations to estimate the power spectrum $S_Y(\omega)$ by inverting the system of equations $S_Y(2k\pi/W) = \sum_m |F_m(2k\pi/W)|^2 \chi_m$, where $\chi_m = \ln(2\hat{p}_m - 1)$, with each control sequence repeated sufficiently many times to achieve an accurate estimate of the survival probability p_m . Note that nonnegative least squares should be used to ensure nonnegativity of the estimated power spectrum. Additionally, in order to reduce sampling error, we did not perform repeated Bernoulli trials to construct \hat{p}_m , instead we took the average of the exact survival probabilities over 1000 independent SchWARMA trajectories.

S.V. SURFACE CODE CIRCUITS

In the main text of the paper, we demonstrate the utility of using SchWARMA to simulate correlated noise processes within a quantum circuit. We compare the SchWARMA approach to a full density matrix simulation of the noisy dynamics. The model that we construct is a system of five qubits. Each has a single qubit Hamiltonian given by:

$$H(t) = \sum_{i=\{x,y,z\}} \eta_i(t) \sigma_i + \Omega(t) (\cos(\phi) \sigma_x + \sin(\phi) \sigma_y), \quad (\text{S37})$$

where $\eta_i(t)$ are zero-mean wide-sense stationary Gaussian processes with correlation functions $\langle \eta_i(\tau) \eta_j(t) \rangle = f_i(|\tau - t|) \delta_{ij}$, ϕ is a user-controlled parameter that specifies the axis of rotation, and $\Omega(t)$ is the time-dependent amplitude of the control pulse. Furthermore, let the η_i have correlation functions given by

$$f_i(\tau) = \frac{\gamma_i}{2\sqrt{\pi}\tau_{c,i}} e^{\frac{-\tau^2}{4\tau_{c,i}^2}}, \quad (\text{S38})$$

where $\tau_{c,i}$ is the correlation time of the noise for axis i and γ_i is the corresponding noise amplitude (see example 2 in the main text for an identical description). Entanglement in the system is generated via a two qubit ZZ entangling operation

$$H(t) = \Omega_{ZZ}^{(k,j)}(t) \sigma_z^{(k)} \otimes \sigma_z^{(j)}, \quad (\text{S39})$$

where $\Omega_{ZZ}^{(k,j)}(t)$ is a controllable coupling term and k and j denote the qubit index.

The standard X and Z check circuits for the surface code are given in Fig. S2: We compile the CNOT into the circuit shown in Fig. S3. The gates are defined as:

$$X = e^{-i\sigma_x\pi/2},$$

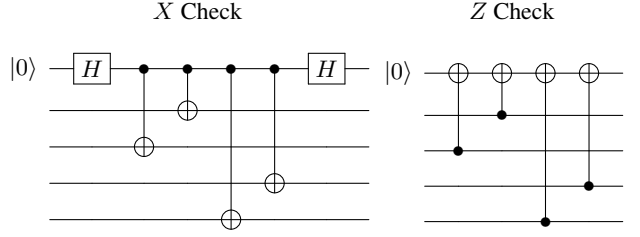


FIG. S2. The X stabilizer is given on the left and the Z stabilizer is given on the right. Measurements of the ancilla are omitted from these circuits.

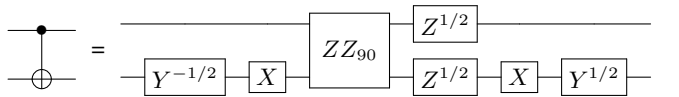


FIG. S3. The CNOT decomposed into elementary gates. The Z rotations are taken to be virtual within all of our simulations and take no time and occur without error.

$$Y^{\pm 1/2} = e^{\mp i\sigma_y\pi/4},$$

$$Z^{1/2} = e^{-i\sigma_z\pi/4},$$

and the controlled ZZ gate between qubits i and j is

$$ZZ_{90} = e^{-i\sigma_z^{(i)} \otimes \sigma_z^{(j)}\pi/4}.$$

For the Z check operator, all the single qubit X and Y rotations between the CNOT gates cancel each other. This allows for a further simplification of the compiled circuit of just single-qubit rotations on the ancilla to start, a sequence of ZZ_{90} gates, followed by single qubit rotations on the ancilla. There are leftover virtual $Z^{1/2}$ gates to be done on the data qubits, but we leave these as they would be virtual and taken care of during the next round of error correction in any system. We chose this gate-set as an exemplar and with the knowledge that it is a commonly seen Hamiltonian in experimental systems.

For the full density matrix simulation, we simulate the entire circuit using a first-order Trotter-Suzuki [S19–S22] approximation to the dynamics. We generate square pulses for each of the gates in our gate-set. We average over different noise realizations and compute for average process map for the entire circuit. An illustrative example is provided in Fig. S4 where we plot the single and two-qubit control pulses for qubit 0 (the top qubit in the circuit diagram) and a single realization of a noise trajectory for the terms in Eqs. (S37) and (S39).

Meanwhile the SchWARMA simulations are much simpler. For them, we do standard circuit simulation where we simply apply the gates as perfect unitary operations and follow them with SchWARMA generated noise after each gate. We average over the same number of noise realizations as in the

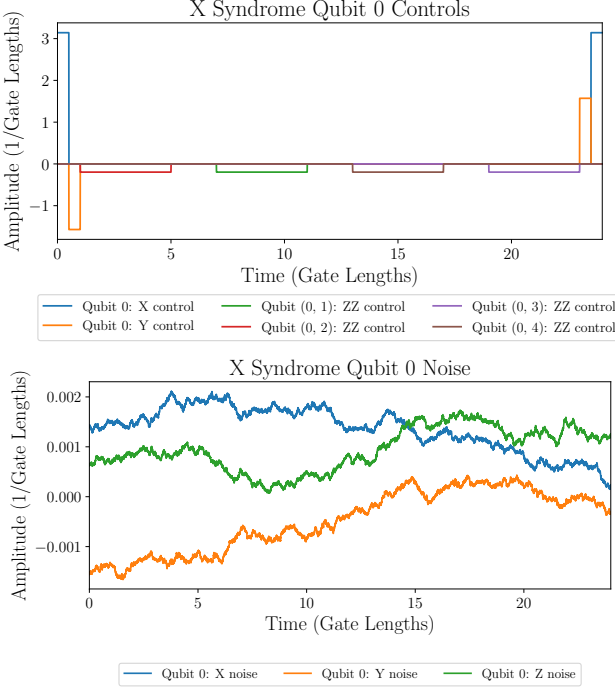


FIG. S4. These two plots provide an illustrative example of how the full simulation of the surface code circuits are done. On the top, we show the single-qubit control amplitudes, $\Omega(t)$, for the Hamiltonian in Eq. (S37) and the two-qubit control amplitudes, $A(t)$, for the Hamiltonian in Eq. (S39). We see single-qubit X and Y controls being applied at the beginning and end of the circuit. These correspond to the application of the Hadamard gate. In the middle, the entangling operations are performed. On the bottom, we plot a single realization of a noise trajectory, $\eta_i(t)$, for the multi-axis noise term in Eq. (S37). We choose noise values $\gamma_x = \gamma_y = \gamma_z = 10^{-4}$ and the correlation time $\tau_{c,x} = \tau_{c,y} = \tau_{c,z} = 32$. Those are in units of inverse gate length and gate length respectively. The noise is always on across the entire duration of the circuit. The upper values yield a highly non-Markovian trajectory.

Trotter-Suzuki simulation method. This does not require generating the full pulse wave forms, as we had to for the Trotter method, yet provides the same circuit level noise model.

S.VI. CONTINUOUSLY DRIVEN SYSTEMS

SchWARMA can be utilized to simulate continuously driven system dynamics in the presence of correlated noise, such as faulty adiabatic dynamics. We demonstrate this by simulating

$$H(t) = H_c(t) + H_e(t), \quad (\text{S40})$$

where $H_c(t)$ generates the pure continuously driven (controlled) dynamics and $H_e(t)$ is the error-generating Hamiltonian. Here, $H_e(t)$ describes a temporally correlated noise process. Generically, we can represent the error Hamiltonian as $H_E(t) = \sum_k \eta_k(t) S_k$ with $\langle \eta_i(t) \eta_j(t') \rangle$ denoting the two-point correlation function for the classical noise process. Note

that S_k are system operators (not necessarily Pauli operators) designating the manner in which the noise affects the system.

Mezze simulations are performed by Trotterizing $H(t)$ as

$$U(T) = \mathcal{T} e^{-i \int_0^T H(t) dt} \approx \prod_{k=1}^{N_T} e^{-i H(k\delta t)\delta t}, \quad (\text{S41})$$

where δt sets the time resolution of the simulation and $N_T = T/\delta t$ denotes the number of time steps. In order to examine the effect of correlated noise on the system, one must average over many trajectories of the noise and therefore, perform this full dynamics simulation numerous times.

SchWARMA simulations are performed by partitioning the controlled dynamics and the correlated noise evolution. The total time evolution is composed of products of ideal evolution followed by SchWARMA-generated noise that effectively captures the effect of $H_e(t)$. More concretely, the evolution is explicitly approximated by

$$U(T) \approx \prod_{j=1}^{N_{sch}} U_E(j\delta t') U_c(j\delta t') U_c^\dagger((j-1)\delta t'), \quad (\text{S42})$$

where $N_{sch} = T/\delta t'$ is the number of SchWARMA time steps, $\delta t' = \kappa \delta t$ is the effective SchWARMA sampling time and

$$U_c(j\delta t') = U_c(j\kappa \delta t) \\ = \mathcal{T} e^{-i \int_0^{j\kappa \delta t} H_c(t) dt} \approx \prod_{k=1}^{j\kappa} e^{-i H_c(k\delta t)\delta t}. \quad (\text{S43})$$

Correlated noise is generated via $U_E(t_j) = \exp(-i \sum_\gamma y_j^{(\gamma)} S_\gamma)$, where the variables $y_j^{(\gamma)}$ are defined by the underlying SchWARMA model and thus, they encapsulate the temporal properties of the noise. Simulating the dynamics in this manner allows one to leverage the noiseless approximation of adiabatic dynamics as a base for the faulty simulations. The noisy dynamics are then captured by averaging a desired metric over realizations of Eq. (S42), where the noise is applied at times $j\delta t'$ that may be much larger than the Trotter time resolution δt .

We consider three different continuously driven systems to demonstrate the efficacy of SchWARMA: (1) a 2-level Landau-Zener system (LZS) [S23, S24], (2) a 3-level LZS [S25], and (3) N -qubit adiabatic Grover's Search [S26]. SchWARMA is shown to be in agreement with full dynamics simulation of each system, while only requiring a fraction of the simulation cost. In the subsequent simulations, $K = 100$; thus, while the ideal simulation cost remains the same, the cost of a noisy simulation is approximately reduced by a factor of 100.

We model the faulty LZ system as

$$H_c(t) = 2\Delta S_x + 2\alpha t S_z \quad (\text{S44})$$

and $H_e(t) = \eta_x(t) S_x$, where S_x and S_z represent spin operators for either the spin-1/2 or spin-1 system. We simulate the dynamics from $t \ll 0$ to $t \gg 0$ to effectively capture the

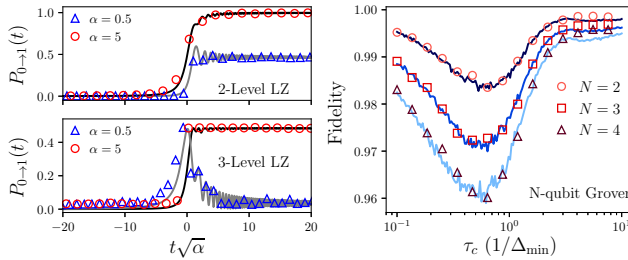


FIG. S5. SchWARMA (symbols) vs. analytical results and full dynamics simulation of continuously driven systems (both shown as solid lines). The comparison indicates good agreement between SchWARMA and alternative approaches. LZ results are shown for a 2-level and 3-level system with noise power $f(0) = 0.003\alpha$ for different driving rates α . Grover's search algorithm comparisons focus on varying correlation time τ_c using a fixed noise power of $f(0) = 0.001\Delta_{\min}^2$.

LZ behavior from $t \rightarrow -\infty$ to $t \rightarrow \infty$ and compare our results to the analytical expressions obtained in Ref. [S27] for the transition probability from $|0\rangle$ to $|1\rangle$ in the presence of slow correlated noise. Fig. S5 conveys that the analytical expression for transition probability as a function of total time is in good agreement with SchWARMA-driven simulations for both systems (1) and (2). The total time, noise correlation time, and noise power are all normalized with respect to the drive strength α for distinct values of $\lambda = \Delta^2/2\alpha$. The total drive time and noise correlation time are given by $T = T_0/\sqrt{\alpha}$ and $\tau_c = \tau_0/\sqrt{\alpha}$, respectively. The normalized times $T_0 = 600$ and $\tau_0 = 100$ are chosen for the simulations shown in Fig. S5. We express the noise power $f(0) = 0.003\alpha$ in terms of the driving rate. Parameter definitions are chosen in accordance with Ref. [S27].

In addition to the LZS, we consider the adiabatic implementation of Grover's search algorithm:

$$H_{ad}(t) = \alpha(t)[I - |+\rangle\langle+|] + (1 - \alpha(t))[I - |m\rangle\langle m|], \quad (\text{S45})$$

where $\alpha(t)$ describes the time-optimal Grover control [S26], $|+\rangle$ denotes the equal superposition state, and $|m\rangle$ represents the target, marked state. The noise is modeled as $H_E(t) = \eta(t) \sum_i \sigma_i^z$; thus, we consider collective dephasing with respect to the computational basis. Simulations shown in Fig. S5 include comparisons between fully Trotterized dynamics and SchWARMA simulations as a function of correlation time with respect to Δ_{\min} , the minimum spectral gap between the ground state and first excited state. The fidelity metric is $F = |\langle \Phi(T) | \psi(T) \rangle|^2$, where $|\Phi(t)\rangle$ denotes the instantaneous ground state of $H_{ad}(t)$ and $\psi(T)$ is the time-evolved state at total time T . The noise power and correlation times are also normalized with respect to Δ_{\min} . The comparisons indicate that SchWARMA is in good agreement with analytical predictions and full dynamics simulations for a variety of N -qubit system sizes.

ACKNOWLEDGEMENTS

We thank Colin Trout, Tim Sweeney, Lorenza Viola, and Leigh Norris for reviewing the manuscript and for fruitful conversations during its preparation. KS, GQ, and PT acknowledge funding from the DOE Office Science contract 4000167418. KS, GQ, PT, and BDC acknowledge funding from the DOE Office of Science Grant Number DE-SC0020316. KS and GQ acknowledge support from ARO MURI grant W911NF-18-1-0218. A portion of this research was supported by the Intelligence Advanced Research Projects Activity via Department of Interior National Business Center contract number 2012-12050800010. The U.S. Government is authorized to reproduce and distribute reprints for Governmental purposes notwithstanding any copyright annotation thereon. The views and conclusions contained herein are those of the authors and should not be interpreted as necessarily representing the official policies or endorsements, either expressed or implied, of IARPA, DoI/NBC, or the U.S. Government.

-
- [S1] “mezze: a toolbox for simulating open quantum system dynamics,” <https://github.com/mezze-team/mezze> (2020).
- [S2] V. Gorini, A. Kossakowski, and E. C. G. Sudarshan, *Journal of Mathematical Physics* **17**, 821 (1976).
- [S3] G. Lindblad, *Communications in Mathematical Physics* **48**, 119 (1976).
- [S4] H.-P. Breuer and F. Petruccione, *The theory of open quantum systems* (Oxford University Press on Demand, 2002).
- [S5] V. Jagadish and F. Petruccione, arXiv preprint arXiv:1902.00909 (2019).
- [S6] C. J. Wood, J. D. Biamonte, and D. G. Cory, *Quantum Information & Computation* **15**, 759 (2015).
- [S7] A. Oppenheim, R. Schafer, and J. Buck, *Discrete-Time Signal Processing* (Prentice Hall, 1999).
- [S8] T. Parks and J. McClellan, *IEEE Transactions on Circuit Theory* **19**, 189 (1972).
- [S9] S.-P. Wu, S. Boyd, and L. Vandenberghe, in *Proceedings of 35th IEEE Conference on Decision and Control*, Vol. 1 (IEEE, 1996) pp. 271–276.
- [S10] S. Plaszczynski, *Fluctuation and Noise Letters* **7**, R1 (2007).
- [S11] P. Stoica and R. L. Moses, *Spectral analysis of signals* (Pearson Prentice Hall Upper Saddle River, NJ, 2005).
- [S12] R. Zimmermann, *SIAM Journal on Matrix Analysis and Applications* **38**, 322 (2017).
- [S13] S. Fiori, *Circuits, Systems, and Signal Processing* **33**, 2449 (2014).
- [S14] S. H. Holan, R. Lund, G. Davis, *et al.*, *Statistics Surveys* **4**, 232 (2010).
- [S15] T. Bollerslev, *Journal of Econometrics* **31**, 307 (1986).
- [S16] L. M. Norris, G. A. Paz-Silva, and L. Viola, *Phys. Rev. Lett.* **116**, 150503 (2016).
- [S17] L. Cywiński, R. M. Lutchyn, C. P. Nave, and S. Das Sarma, *Phys. Rev. B* **77**, 174509 (2008).

- [S18] G. A. Paz-Silva and L. Viola, *Phys. Rev. Lett.* **113**, 250501 (2014).
- [S19] M. Suzuki, *Communications in Mathematical Physics* **51**, 183 (1976).
- [S20] M. Suzuki, *Communications in Mathematical Physics* **57**, 193 (1977).
- [S21] M. Suzuki, *Journal of Mathematical Physics* **26**, 601 (1985).
- [S22] M. Suzuki, *Physics Letters A* **146**, 319 (1990).
- [S23] L. Landau, *Phys. Z Sowjetunion* **2** (1932).
- [S24] C. Zener, *Proc. R. Soc. London, Ser. A* **137** (1932).
- [S25] C. E. Carroll and F. T. Hioe, *Journal of Physics A: Mathematical and General* **19**, 2061 (1986).
- [S26] J. Roland and N. J. Cerf, *Phys. Rev. A* **65**, 042308 (2002).
- [S27] M. B. Kenmoe, H. N. Phien, M. N. Kiselev, and L. C. Fai, *Phys. Rev. B* **87**, 224301 (2013).